Makara Journal of Science

Volume 24
Issue 2 *June*

Article 7

6-26-2020

Improving the Surface Corrosion Resistance of AMX601 Magnesium Alloy by Acid–Alkaline Treatment

Anawati Anawati
Department of Physics, Faculty of Mathematics and Natural Sciences, Universitas Indonesia, Depok 16424, Indonesia, anawati@sci.ui.ac.id

Hidetaka Asoh
Department of Applied Chemistry, Kogakuin University, 2665-1 Nakano, Hachioji, Tokyo 192-0015, Japan

Sachiko Ono
Department of Applied Chemistry, Kogakuin University, 2665-1 Nakano, Hachioji, Tokyo 192-0015, Japan

Improving the Surface Corrosion Resistance of AMX601 Magnesium Alloy by Acid–Alkaline Treatment

Cover Page Footnote

We acknowledge Hibah Kompetitif Nasional Penelitian Tesis Magister (PTM) Dikti (Contract No. NKB-1894/UN2.R3.1/HKP.05.00/2019) for supporting this research.

Makara Journal of Science, 24/2 (2020), 112–118
doi: 10.7454/mss.v24i1.11910

Improving the Surface Corrosion Resistance of AMX601 Magnesium Alloy by Acid–Alkaline Treatment

Anawati[1*], Hidetaka Asoh[2] and Sachiko Ono[2]

1. Department of Physics, Faculty of Mathematics and Natural Sciences, Universitas Indonesia, Depok 16424, Indonesia
2. Department of Applied Chemistry, Kogakuin University, 2665-1 Nakano, Hachioji, Tokyo 192-0015, Japan

[*]*E-mail: anawati@sci.ui.ac.id*

Received September 11, 2019 | Accepted June 9, 2020

Abstract

A drawback of acid cleaning as surface finishing of magnesium (Mg) surface is the absence of a protective oxide film on its surface. Acid–alkaline treatment is proposed to enhance the surface corrosion resistance of AMX601 Mg alloy. Acid–alkaline treatment was conducted by first dipping the alloy in HNO_3–H_3PO_4 solution and then immersing the alloy in NaOH solution. The potentiodynamic polarization test in 0.9% NaCl solution at 37 °C revealed a nobler corrosion potential of −1.36 $V_{Ag/AgCl}$ and a lower corrosion current density of 36.0 $\mu A \cdot cm^{-2}$ of the acid–alkaline-treated specimen than the acid-treated (−1.44 $V_{Ag/AgCl}$, 89.7 $\mu A \cdot cm^{-2}$) and untreated (−1.52 $V_{Ag/AgCl}$, 40.0 $\mu A \cdot cm^{-2}$) specimens. Acid treatment induced a significantly higher surface roughness (20 μm) than acid–alkaline (10 μm) and grinding (0.5 μm) treatments because of the selective dissolution of the Mg matrix and the accumulation of intermetallic precipitates. The film formed on the acid–alkaline-treated specimen was thick and free of cracks, whereas that formed on the acid-treated specimen was thin and cleaved. The formation of a protective oxide film and the enrichment of cathodic intermetallic particles on the acid–alkaline-treated specimen enhanced the corrosion resistance of the surface.

Keywords: magnesium, corrosion, chemical treatment, GDOES, SEM

Introduction

Over the years, there has been a constant interest in expanding the application of magnesium (Mg) alloys as biodegradable implant materials. Mg and its alloys exhibited suitable mechanical properties, spontaneous degradation, and high biocompatibility [1,2]. A study of Mg stent implanted in human coronary arteries for 4 months proved the excellent biocompatibility of Mg as no allergic reaction was observed and complete degradation of Mg was achieved without adverse effects [3]. However, a slow degradation rate in the early implantation period is required to avoid the formation of subcutaneous gas and preserve implant integrity.

The natural oxide film formed on the Mg surface is composed of three layers, namely, a hydrated inner layer, a dense dehydrated intermediate layer, and the outermost layer with a platelet-like morphology [4]. However, the natural oxide film is not protective and is easily destabilized by a corrosive solution. Surface treatment is considered the simplest method to improve the corrosion resistance of metal surfaces. The traditional surface treatment applied to metals typically uses the chromate bath solution [5]. Chrome-based solutions are not used as a biomaterial because the hexavalent chrome is toxic and dangerous for the environment. Some inorganic acids have been used as bath solutions for the surface treatment of Mg alloys [6–11]. The use of hydrochloric acid (HCl) to treat AZ91 and AM50 alloys before the final coating showed an improvement in both coating adhesion and corrosion resistance of the alloy [6]. HCl treatment promoted the enrichment of the β phase and eutectic α, as well as aluminum (Al), on the surface. The rough and oxidized surface was beneficial to the improvement of the uniformity and thickness of the final coating. The incorporation of Al in the magnesium oxide film as a result of acid treatment improved the barrier properties of the magnesium oxide film. The treatment of AZ61 alloy using a solution containing $Zn(NO_3)_2$ and stearic acid resulted in a phosphate/ZnO multilayer, with a controllable corrosion rate depending on the number of multilayers [8]. The growth of the Mg–Al layered double hydroxide enhanced the corrosion protection of Mg alloys by enhancing the hydrophobicity of the surface [9,10]. Most of the reported works [6–11] used an acid solution as surface treatment to improve surface resistance. In this work, final treatment in an alkaline solution was performed after acid treatment to obtain a protective oxide film on AMX601

Mg alloy. From the thermodynamic viewpoint, the formation of a stable magnesium oxide/hydroxide occurs only in an alkaline environment. The corrosion resistance of an acid–alkaline-treated surface compared with that of an acid-treated surface was analyzed by polarization tests in 0.9% NaCl solution.

Experimental Method

The specimen used in this study is a rolled plate commercial AMX601 Mg alloy composed of the following alloying elements: Al 6 wt%, Mn 0.26 wt%, and Ca 1 wt%. The plate with a thickness of 1 mm was cut to yield a square working area of 1.5 cm × 1.5 cm. The specimen was degreased in acetone and ethanol consecutively in an ultrasonic bath for 3 min.

Surface treatment. The microstructure and corrosion behavior of the AMX601 specimens were investigated by preparing three sets of specimens. The first set of specimens was mechanically ground with #600, #800, #1000, and #2000 grit paper under running water. The ground specimen was used as the standard. After grinding, the specimen was first cleaned in deionized (DI) water in an ultrasonic bath at room temperature to remove debris and then dried. The second set of specimens was ground and chemically treated in a mixed acid solution of 8 vol% HNO_3–1 vol% H_3PO_4 for 20 s at 25 °C, which was designated as acid treatment. The third set of specimens was treated in acid–alkaline solution by soaking the ground specimen first in acid solution and then in 5 wt% NaOH solution at 80 °C for 1 min. After the chemical treatments, the specimen was first washed thoroughly with DI water and then dried. The procedure for acid–alkaline treatment used in previous research was utilized as pretreatment for the growth of composite conversion coatings [12–14].

Surface characterization. The surface microstructure was investigated by scanning electron microscopy (SEM), and the elemental distribution was analyzed by energy-dispersive X-ray spectroscopy (EDS; JEOL EX-54175JMU, JEOL, Ltd., Tokyo, Japan). The surface of the specimen was previously subjected to Pt/Pd sputtering to reduce charging under electron beam exposure. Observation of the surface roughness was done using a laser microscope (Olympus, Tokyo, Japan). To investigate the elemental distribution on the surface layer, elemental depth profile analysis of a circular area (with a diameter of 4 mm) of the alloy surface was performed using glow discharge optical emission spectroscopy (GDOES; Jobin-Yvon JY5000RF, Horiba, Ltd., Kyoto, Japan).

Corrosion test. The effect of various surface treatments on the corrosion behavior of AMX601 specimens was investigated by performing electrochemical polarization tests in 0.9% NaCl solution at 37 °C based on the ASTM standards [15]. The potential was swept from −1.65 $V_{Ag/AgCl}$ to −1.25 $V_{Ag/AgCl}$, with a scan rate of 0.1 mV/s, using an Ivium potentiostat. Before measurement, the specimen was immersed in the test solution for 20 min to stabilize the open circuit potential. Three electrode configurations were employed, with Pt as the counter electrode and Ag/AgCl as the reference electrode. The specimen itself was set as the working electrode. The polarization data were analyzed by the Tafel extrapolation method to determine the corrosion potential and corrosion current density.

Results and Discussion

Observation in the laboratory revealed that the ground specimen exhibited a smooth metallic surface. Rolling lines were no longer visible on the ground surface. Acid treatment generated a clean metallic surface with an increasing degree of metallic reflection. During acid treatment, rapid dissolution of the metal surface occurred, as indicated by the robust release of hydrogen gas to the solution. The subsequent alkaline treatment turned the metal surface to matte white because of the formation of the oxide/hydroxide layer.

The surface morphology of the specimens after the treatments was investigated using a scanning electron microscope and a laser microscope. Figures 1a-1c shows the SEM images of the AMX601 surface after the treatments and Figures 1d-1f are the corresponding topography captured by the laser microscope. The mechanically ground surface exhibited a smooth uniform morphology with some grinding scratches (Figure 1a). The surface was relatively flat and exhibited a contrast of green and yellow colors in Figure 1d, which corresponded to the surface roughness of 0.5 μm. The surface became significantly rough after acid treatment, as shown in Figure 1b. Enrichment of precipitates was observed in the form of both continuous and discrete particles, which increased the surface roughness significantly to 20 μm (Figure 1e). The surface exhibited a contrast of blue, green, and red colors. Most of the particles were located in the outer layer, as depicted by the red color in the image. The precipitates were not attacked by the acid solution. A previous work [12] had shown that the precipitates in AMX601 mainly consisted of β and Al_2Ca phases, which were more cathodic than the Mg matrix. Acid treatment selectively dissolved the Mg matrix, resulting in the green and blue colors in the image. The matrix was dissolved deeper along the rolling direction, resulting in a groove structure, as depicted by the blue color in the image. Thermodynamically, Mg is a reactive metal with a low potential at −2.36 V [5]. The potential–pH diagram of Mg in water indicated that the alloy is unstable in both neutral and acidic environments [16]. Corrosion was considerably accelerated in solutions with low pH, thereby dissolving the surface layer. The subsequent alkaline

treatment reduced the surface roughness, as displayed in Figs. 1c and 1f. The number of intermetallic precipitates on the surface of the alkaline-treated specimen increased and elongated relative to the acid-treated specimen. The topography illustrated in Figure 1f shows the color variation of green and red corresponding to the surface roughness of 10 µm. Alkaline treatment reduced the surface roughness to half of that of acid treatment.

The elemental composition of the surface after the treatments was analyzed by EDS. Figures 2, 3, and 4 show the SEM images and the corresponding EDS maps of the surface after grinding, acid treatment, and acid–alkaline treatment, respectively. Grinding is a common surface treatment for most metals to refine the metal surface and remove dirt and debris during manufacturing. Few grinding lines that cross each other were observed in the SEM image shown in Figure 2a. Some spherical intermetallic particles were distributed on the surface and appeared brighter than the surrounding matrix. Some of the intermetallic particles were distributed next to each other, forming a line. The reticular distribution preferentially formed along the grain boundaries that exhibited low energy. Such a network arrangement is beneficial to the prevention of corrosion propagation along the grain boundaries [17]. The EDS maps illustrated in Figs. 2b to 2e show that the intermetallic particles mainly contained Mg, Ca, and Al, as confirmed by the strong signal in their maps. The composition of the intermetallic particles consisted mainly of Al_2Ca and a small number of Mg_2Ca, in addition to the β ($Mg_{17}Al_{12}$) phase.

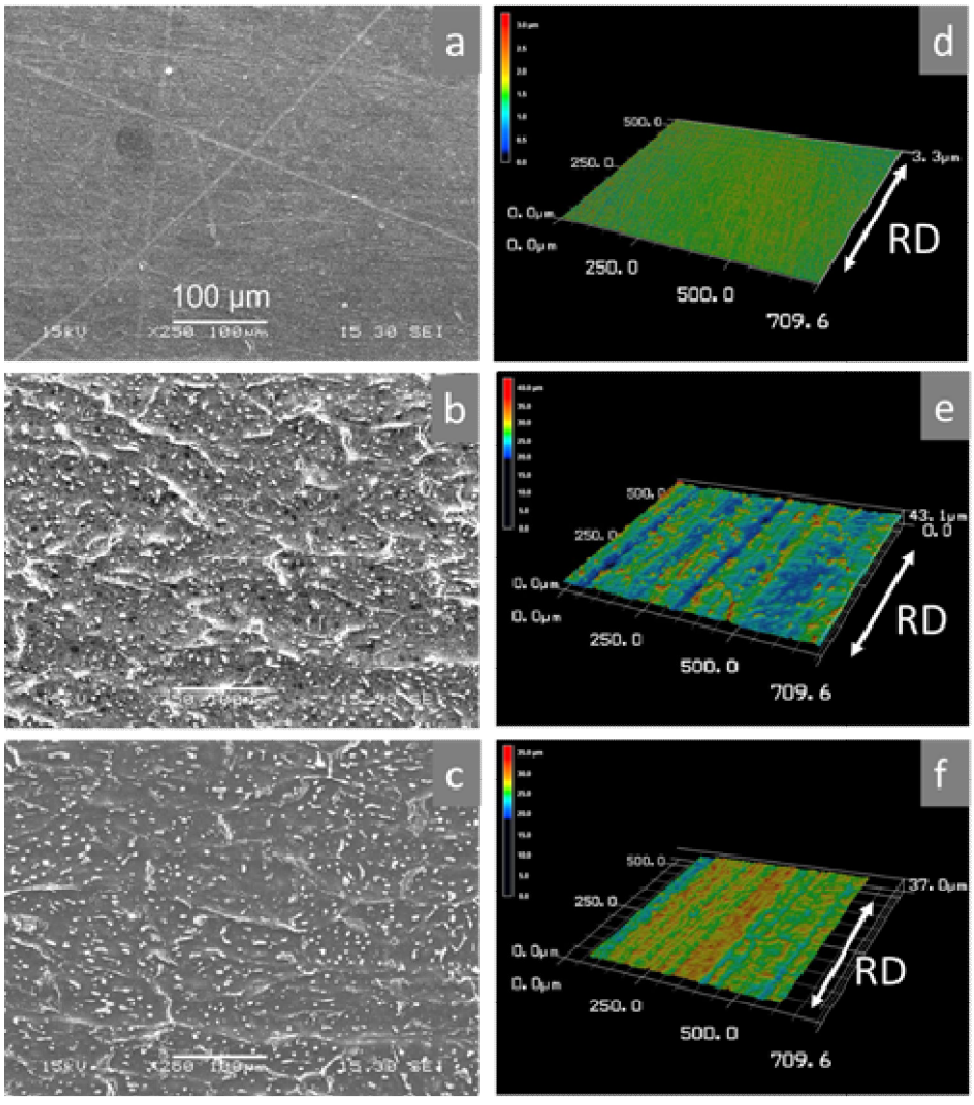

Figure 1. SEM Images of the Surface After (a) Grinding, (b) Acid Treatment, and (c) Acid–alkaline Treatment and (d)–(f) the Corresponding Surface Roughness

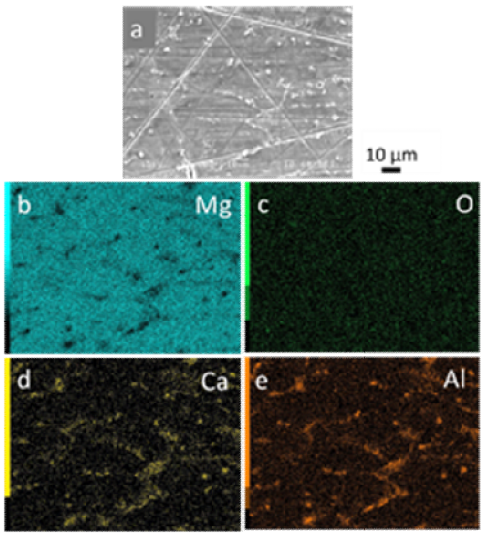

Figure 2. (a) SEM Image and (b)–(e) the Corresponding EDS Maps of Mg, O, Ca, and Al of the Ground AMX601 Surface

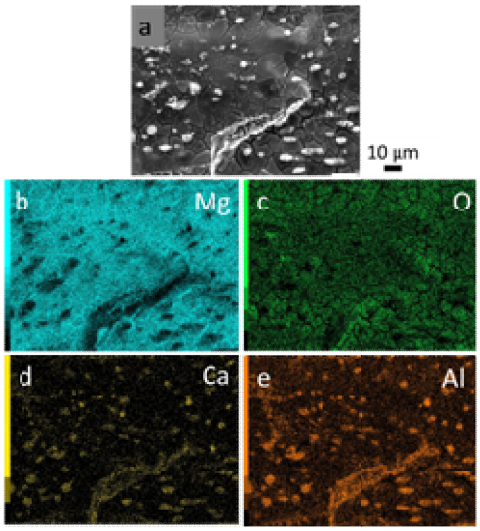

Figure 3. (a) SEM Image and (b)–(e) the Corresponding EDS Maps of Mg, O, Ca, and Al of the Acid-treated AMX601 Surface

The intermetallic particles formed on the surfaces of acid-treated and acid–alkaline-treated specimens were larger than that of ground specimens, as shown in Figs. 3 and 4. The fine particles that appeared on the ground specimen were approximately 1 µm size, whereas those that appeared on the acid-treated specimen were approximately 5 µm and those that appeared on the acid–alkaline-treated specimen were elongated with the size of approximately 10 µm. Similarly, the continuous intermetallic particles were distributed along the radial direction. The chemical treatments in both acid and alkaline solutions increased the intermetallic particle size. The unavoidable accumulation of intermetallic particles occurred as a result of treatment in an acid bath solution [6,11]. The chemical treatments also induced the formation of oxide layers on the surfaces, as indicated by the strong O signal in Figure 3c and 4c relative to that shown in the maps of the ground specimens (Figure 2c). The oxide films formed on both acid-treated and acid–alkaline-treated specimens contained Al. The incorporation of Al in the oxide layer contributed to the increase in the corrosion resistance of the surface [17]. The film formed on the acid-treated surface was cleaved (Figure 3a), whereas that formed on the acid–alkaline-treated surface was free of cracks (Figure 4a). The cleaved structure observed on the surface of the acid-treated specimen (Figure 3a) was likely due to hydration of the oxide. The film formed after acid–alkaline treatment was thicker than that formed after acid treatment only, as revealed in the O map, which was brighter for the acid–alkaline-treated specimen than the acid-treated specimen. Moreover, the Al and Ca signals from the particles in the map of the acid–alkaline-treated specimen were not as strong as that in the map of the acid-treated specimen. The intermetallic particles were covered by the thick oxide film formed during alkaline treatment.

Figure 5 shows the results of the quantitative analysis of the EDS maps illustrated in Figs. 2 to 4. The results clearly showed that the oxide films on the acid-treated and acid–alkaline-treated specimens were thicker, as indicated by the O concentrations, than that on the ground specimen. The enrichment of intermetallic precipitates on the acid-treated specimen contributed to the high concentration of Al detected on its surface. The film formed on the acid-treated surface contained P, which was derived from the acid solution, whereas the film formed on the acid–alkaline-treated surface was purely composed of Mg–O.

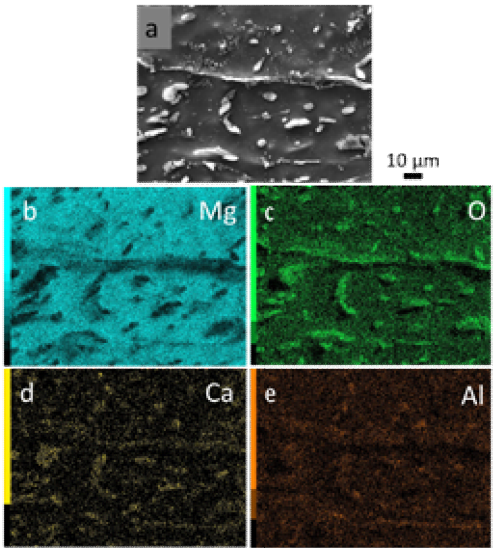

Figure 4. (a) SEM Image and (b)–(e) the Corresponding EDS Maps of Mg, O, Ca, and Al of the Acid–alkaline-treated AMX601 Surface

Confirming the results of the EDS analysis, the GDOES depth profile analysis showed a thin oxide layer on the ground AMX601 specimen, whereas a relatively thicker oxide layer was observed on the acid-treated surface and further thickening of the oxide layer was observed on the acid–alkaline-treated surface, as shown in Figure 6. The oxide–metal interface was indicated by the dashed line. The interface was defined as the cross point where the O profile decreased and the Mg profile increased. The metal part of the ground specimen was reached after only 5 s sputtering from the surface, as indicated by the sudden increase in the Mg signal and the decrease in the O signal. Meanwhile, the acid-treated specimen required the sputtering time of 25 s, which is five times longer, to reach the oxide–metal interface and the acid–alkaline-treated specimen required the sputtering time of 38 s to reach the metal part. Moreover, the acid–alkaline-treated specimen exhibited the highest O profile intensity, followed by the acid-treated specimen. Meanwhile, the ground specimen exhibited the lowest O profile intensity. This finding proved that the thickness of the oxide layer followed the order: grinding < acid treatment < acid–alkaline treatment. The oxide layer formed on the ground specimen contained only Mg and O. Meanwhile, enrichment of Al and Ca was detected on the oxide layer formed on both acid-treated and acid–alkaline-treated surfaces. This finding is consistent with the EDS results that showed enrichment of Al and Ca as intermetallic particles on the surface of acid-treated and acid–alkaline-treated specimens. The P ions from the acid solution were incorporated in the oxide layer, as confirmed by the high intensity of P in the oxide layer, which then decreased significantly upon reaching the bulk metal. The intensity of P in the acid–alkaline-treated specimen was lower than that in the acid-treated specimen. The P-containing layer, which was formed during acid treatment, was buried in freshly formed oxide as a result of the final alkaline treatment.

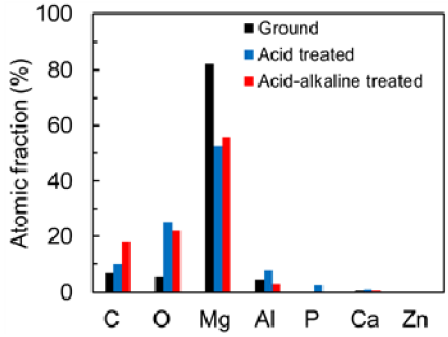

Figure 5. Atomic Fraction of the Elements on the AMX601 Surface after Grinding, acid Treatment, and Acid–alkaline Treatment

The potentiodynamic polarization curves of the AMX601 specimen subjected to a variety of surface treatments are displayed in Figure 7. The corrosion potentials and corrosion current densities are listed in Table 1. The corrosion potential of the AMX601 Mg alloy varied depending on the applied surface treatment. The corrosion current density also varied but still within an order of magnitude. The chemical treatment ennobled the corrosion potential of the ground specimen significantly. The acid treatment shifted the corrosion potential of the alloy by approximately 90 mV to a positive value, and further ennoblement of approximately 170 mV was observed in the acid–alkaline-treated specimen. The corrosion potential of the AMX601 surface was affected by the oxide film resistance, which depended on the thickness and composition of the film. The oxide film formed as a result of acid–alkaline treatment was thicker and, therefore, more protective than that formed as a result of acid treatment only. The oxide layer served as a barrier between the metal surface and the corrosive solution. Once a protective oxide layer was developed on the metal surface, surface passivation was achieved. A stable $Mg(OH)_2$ film was obtained after treatment in the alkaline solution having a pH >11 [16]. The volume fraction of the intermetallic particles on the surface influenced the corrosion potential. The high volume-fraction of the intermetallic particles, which had a more positive potential than the matrix, tended to increase the corrosion potential of the surface [17]. As

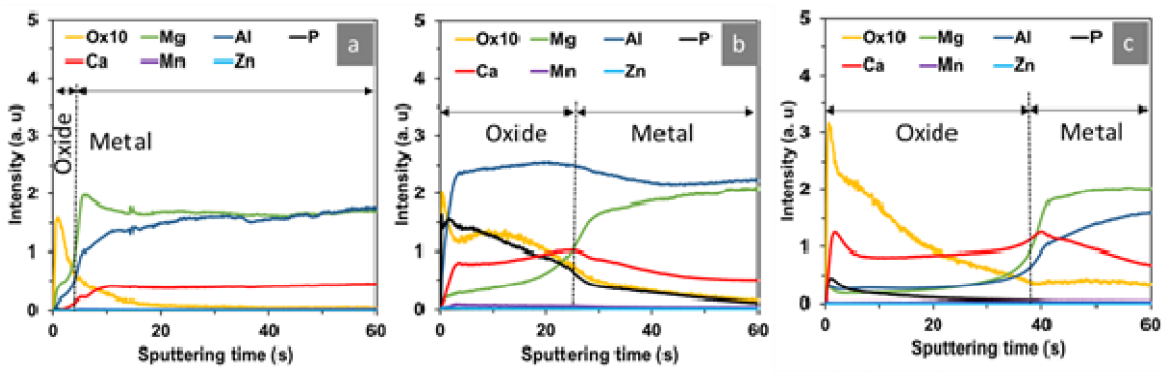

Figure 6. GDOES Depth Profile Analysis of (a) Ground, (b) Acid-treated, and (c) Acid–alkaline-treated AMX601 Specimen

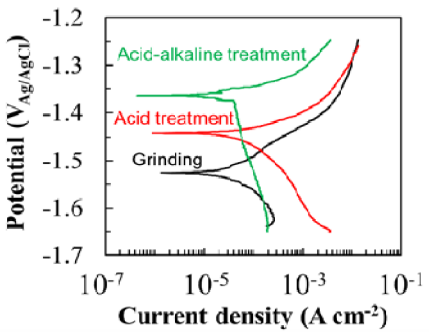

Figure 7. Polarization Curves of Ground, Acid-treated, and Acid–alkaline-treated AMX601 Mg Alloy

Table 1. Corrosion Potentials and Corrosion Current Densities of the AMX601 Specimens Derived from the Polarization Curves Shown in Figure 7

Surface treatment	E_{corr} ($V_{Ag/AgCl}$)	i_{corr} (A·cm^{-2})
Grinding	−1.52	4.00×10^{-5}
Acid treatment	−1.44	8.97×10^{-5}
Acid–alkaline treatment	−1.36	3.60×10^{-5}

shown in Figure 7, the polarization measurements of the AMX601 specimen indicated that the cathodic current densities of the acid-treated specimen were twice that of the ground specimen. By contrast, acid–alkaline treatment resulted in lower cathodic current densities (green curve in Figure 7) than grinding. Although the intermetallic particles were larger after acid–alkaline treatment than after acid treatment only, the oxide layer that covered the specimen after acid–alkaline treatment was thicker than that after acid treatment (Figure 6). The oxide layer was thick enough to act as a barrier that prevents the corrosion reaction on the surface. In other words, the surface resulting from acid–alkaline treatment was electrochemically passive up to the breakdown potential of −1.36 $V_{Ag/AgCl}$. Alkaline treatment following acid pickling was proved to significantly improve the corrosion resistance of the Mg alloy surface.

Conclusion

The effect of chemical treatments on the corrosion resistance of AMX601 Mg alloys has been investigated by conducting potentiodynamic polarization tests. An improvement in corrosion resistance was exhibited by the acid-treated and acid–alkaline-treated specimens. The corrosion potentials of the ground specimen became 90 and 170 mV nobler as a result of acid and acid–alkaline treatments, respectively. Meanwhile, the corrosion current densities were within the same order of magnitude. The results of EDS and GDOES depth profile analyses showed that the improvement in corrosion resistance was due to the formation of the protective oxide/hydroxide layer and the ennoblement of the cathodic intermetallic particles on the surface. The oxide layer formed after acid–alkaline treatment was thicker than that after acid treatment only. The volume fraction of intermetallic particles observed on the surface as a result of acid–alkaline treatment was also higher than that as a result of acid treatment. The combination of a thick oxide layer and a high volume-fraction of intermetallic particles in the acid–alkaline-treated specimen led to the improvement in corrosion resistance of the surface.

Acknowledgements

We acknowledge Hibah Kompetitif Nasional Penelitian Tesis Magister (PTM) Dikti (Contract No. NKB-1894/UN2.R3.1/HKP.05.00/2019) for supporting this research.

References

[1] DeGarmo, E.P., Black, J.T., Kohser, R.A. 2007. Materials and processes in engineering, 10th ed., Wiley.

[2] Witte, F., Hort, N., Vogt, C., Cohen, S., Ulrich, K., Willumeit, R., Feyerabend, F. 2008. Current Opinion in Solid State and Materials Science Degradable biomaterials based on magnesium corrosion. Curr. Opin. Solid State Mater. Sci. 12: 63–72, http://dx.doi.org/10.1016/j.cossms.2009.04.001.

[3] Waksman, R., Erbel, R., Di Mario, C., Bartunek, J., de Bruyne, B., Eberli, F.R., Erne, P., Haude, M., Horrigan, M., Ilsley, C., Böse, D., Bonnier, H., Koolen, J., Lüscher, T.F., Weissman, N.J. 2009. Early- and Long-Term Intravascular Ultrasound and Angiographic Findings After Bioabsorbable Magnesium Stent Implantation in Human Coronary Arteries. JACC Cardiovasc. Interv. 2: 312–320, http://dx.doi.org/10.1016/j.jcin.2008.09.015.

[4] Nordlien, J.H., Ono, S., Masuko, N., Nisancioglu, K. 1997. A tem investigation of naturally formed oxide films on pure magnesium. Corros. Sci. 39: 1397–1414, http://dx.doi.org/10.1016/S0010-938X(97)00 037-1.

[5] Pekguleryuz, M., Kainer, K., Kaya, A. 2013. Fundamentals of Magnesium Alloy. Woodhead Publishing Ltd., Cambridge, UK.

[6] Brunelli, K., Dabalà, M., Calliari, I., Magrini, M. 2005. Effect of HCl pre-treatment on corrosion resistance of cerium-based conversion coatings on magnesium and magnesium alloys. Corros. Sci. 47: 989–1000, http://dx.doi.org/10.1016/j.corsci.2004.06.016.

[7] Ximei, W., Liqun, Z., Huicong, L., Weiping, L. 2008. Influence of surface pretreatment on the anodizing film of Mg alloy and the mechanism of

the ultrasound during the pretreatment. Surf. Coatings Technol. 202: 4210–4217, http://dx.doi.org/10.10 16/j.surfcoat.2008.03.018.

[8] Yuan, J., Yuan, R., Wang, J., Li, Q., Xing, X., Liu, X., Hu, W. 2018. Fabrication and corrosion resistance of phosphate/ZnO multilayer protective coating on magnesium alloy. Surf. Coatings Technol. 352: 74–83, http://dx.doi.org/10.1016/ j.sur fcoat.2018.07.090.

[9] Zhang, G., Wu, L., Tang, A., Chen, X.B., Ma, Y., Long, Y., Peng, P., Ding, X., Pan, H., Pan, F. 2018. Growth behavior of MgAl-layered double hydroxide films by conversion of anodic films on magnesium alloy AZ31 and their corrosion protection. Appl. Surf. Sci. 456: 419–429, http://dx.doi.org/10.101 6/j.apsusc.2018.06.085.

[10] Yao, Q.S., Zhang, F., Song, L., Zeng, R.C., Cui, L.Y., Li, S.Q., Wang, Z.L., Han, E.H. 2018. Corrosion resistance of a ceria/polymethyl trimethoxysilane modified Mg-Al-layered double hydroxide on AZ31 magnesium alloy. J. Alloys Compd. 764: 913–928, http://dx.do i.org/10.1016/ j.jallcom.2018.06.152.

[11] Jiang, S., Cai, S., Zhang, F., Xu, P., Ling, R., Li, Y., Jiang, Y., Xu, G. 2018. Synthesis and characterization of magnesium phytic acid/apatite composite coating on AZ31 Mg alloy by microwave assisted treatment. Mater. Sci. Eng. C. 91: 218–227, http://dx.doi.org/10.1016/j.msec.2018. 05.041.

[12] Anawati, A., Asoh, H., Ono, S. 2017. Effects of alloying element ca on the corrosion behavior and bioactivity of anodic films formed on AM60 mg alloys. Materials (Basel). 10, http://dx.doi.org/10.3 390/ma10010011.

[13] Anawati, A., Asoh, H., Ono, S. 2018. Degradation Behavior of Coatings Formed by the Plasma Electrolytic Oxidation Technique on AZ61 Magnesium Alloys Containing 0, 1 and 2 wt% Ca. Int. J. Technol. 9: 622, http://dx.doi.org/10.147 16/ijtech.v9i3.712.

[14] Ono, S., Moronuki, S., Mori, Y., Koshi, A., Liao, J., Asoh, H. 2017. Effect of Electrolyte Concentration on the Structure and Corrosion Resistance of Anodic Films Formed on Magnesium through Plasma Electrolytic Oxidation. Electrochim. Acta. 240: 415–423, http://dx.doi.org/10.1016/ j.electacta.201 7.04.110.

[15] Channing, S. 1991. Annual Book of ASTM Standards: ASTM International. Conshohocken, PA, USA.

[16] Pourbaix, M. 1966. Atlas of Electrochemical Equilibria in Aquaeous Solution. Pergamont Press, Oxford, New York.

[17] Lunder, O., Nordien, J.H., Nisancioglu, K. 1997. Corrosion Resistance of Cast Mg-Al Alloys. Corros. Rev. 15: 439–470, http://dx.doi.org/ 10.1515/COR RREV.1997.15.3-4.439.